Dalton Transactions

ROYAL SOCIETY OF CHEMISTRY

PAPER

View Article Online
View Journal | View Issue

Open Access Article. Published on 25 August 2023. Downloaded on 1/9/2026 1:16:45 PM.
This article is licensed under a Creative Commons Attribution-NonCommercial 3.0 Unported Licence.

Check for updates

Cite this: *Dalton Trans.*, 2023, **52**, 13089

Importance of isothermal titration calorimetry for the detection of the direct binding of metal ions to mismatched base pairs in duplex DNA†

Hidetaka Torigoe * and Fumihiro Arakawa

Received 30th June 2022,
Accepted 23rd August 2023

DOI: 10.1039/d2dt02097a

rsc.li/dalton

Metal ion–nucleic acid interactions contribute substantially to the structure and biological activity of nucleic acids and have a wide range of potential applications in nanotechnology. In this study, we examined the interactions between metal ions and mismatched base pairs in duplex DNA to reveal the underlying molecular mechanism. UV melting analyses showed that the melting temperature (T_m) of a 21-base pair duplex DNA with each of the C–A, C–C and C–T mismatched base pairs increased upon the addition of Ag^+. However, isothermal titration calorimetry (ITC) demonstrated that Ag^+ only bound to the C–C mismatched base pair of the duplex DNA to form C–Ag–C bonds, without binding to the C–A and C–T mismatches. These results showed that T_m increased even when metal ions did not bind to the mismatched base pairs of the duplex DNA. Although the increase in T_m upon the addition of the metal ions is often used to detect metal ion binding to mismatched base pairs of duplex DNA, these results indicated that UV melting analyses are unable to detect the direct binding of metal ions to the mismatched base pairs. Because ITC analyses directly detect the heat derived from metal ion binding to mismatched base pairs of duplex DNA, we concluded that this may be an effective detection approach.

Introduction

Binding between metal ions and nucleic acids contributes to the structure and folding of nucleic acids, attenuation of electrostatic repulsion among nucleic acid phosphate backbones,[1–3] and the biological functions of nucleic acids, such as enzymatic activity of ribozymes and DNAzymes.[4,5] This binding also has a wide range of potential applications for nanotechnology, such as the development of biomolecular nanomaterials, nanomachines and nanodevices.[6–8]

The structural and thermodynamic properties of binding to duplex DNA with only perfectly matched base pairs have been studied for many metal ions, such as Cr^{3+},[9] Cr^{6+},[9] Tl^+,[10] Fe^{2+},[11] Fe^{3+},[11] Al^{3+},[12] Cd^{2+},[13] and Mn^{2+}.[14] Recently, the binding between a metal ion, Hg^{2+}, and duplex DNA with a mismatched base pair has also been analyzed.[15–22] UV melting analyses have shown that the melting temperature (T_m) of duplex DNA with a T–T mismatched base pair increased significantly in response to Hg^{2+} addition,[15,16,18] with no significant change for the corresponding duplex DNA with perfectly matched base pairs or other mismatched base pairs.[18] No significant increase in the T_m of the duplex DNA with the T–T mismatched base pair was observed upon the addition of other metal ions (Mg^{2+}, Ca^{2+}, Mn^{2+}, Fe^{2+}, Fe^{3+}, Co^{2+}, Ni^{2+}, Cu^{2+}, Zn^{2+}, Ru^{3+}, Pd^{2+}, Ag^+, Cd^{2+}, and Pb^{2+}).[15,16] Thus, the increase in the T_m of the duplex DNA with the T–T mismatch upon the addition of Hg^{2+} was quite specific. The T_m value of the duplex DNA with the T–T mismatched base pair upon the addition of Hg^{2+} was comparable to that with the corresponding T–A or A–T perfectly matched base pair. Isothermal titration calorimetry (ITC)[23] has shown that Hg^{2+} binds directly to the T–T mismatched base pair in duplex DNA at a molar ratio of 1 : 1 with a binding constant on the order of 10^5 M^{-1} to form a T–Hg–T base pair.[18,20] The direct binding of Hg^{2+} increased the T_m value of the duplex DNA with the T–T mismatched base pair.

The interaction between another metal ion, Ag^+, and duplex DNA with a mismatched base pair has been examined.[19,22,24–30] The increase in the T_m of a mismatched base pair duplex DNA was observed upon Ag^+ addition.[24,26,30] The T_m values of duplex DNA with each of the C–A, C–C and C–T mismatched base pairs increased upon the addition of Ag^+, although the magnitude of the increase was the highest in the case of the C–C mismatched base pair. The increase in the T_m is often used to detect the direct binding of metal ions to mismatched base pairs.[31–38] However, it is not clear whether the increase in the T_m values of duplex DNA with the C–A, C–C

Department of Applied Chemistry, Faculty of Science, Tokyo University of Science, 1-3 Kagurazaka, Shinjuku-ku, Tokyo 162-8601, Japan. E-mail: htorigoe@rs.tus.ac.jp; Fax: +81-3-5261-4631; Tel: +81-3-5228-8259

† Electronic supplementary information (ESI) available. See DOI: https://doi.org/10.1039/d2dt02097a

Open Access Article. Published on 25 August 2023. Downloaded on 1/9/2026 1:16:45 PM.
This article is licensed under a Creative Commons Attribution-NonCommercial 3.0 Unported Licence.

or C–T mismatched base pairs upon the addition of Ag^+ indicates the direct binding of the metal ions to the mismatched base pairs. In the present study, we performed ITC analyses to examine whether Ag^+ directly binds to each of the C–A, C–C and C–T mismatched base pairs in duplex DNA to form C–Ag–A, C–Ag–C and C–Ag–T metal-mediated base pairs. Unexpectedly, ITC results revealed that Ag^+ is unable to bind to C–A and C–T mismatched base pairs, but binds directly to the C–C mismatched base pair in the duplex DNA to form a C–Ag–C metal-mediated base pair. We discuss the reason why Ag^+ was unable to bind to the C–A and C–T mismatched base pairs in duplex DNA, despite the increase in T_m upon the addition of Ag^+.

Experimental section

Preparation of oligonucleotides

We synthesized 21-mer complementary DNA oligonucleotides, F21**X** (5′-d(GCCCATTGGA**X**TGACGCTCTG)-3′) (**X** = A, C, G and T) (Fig. 1) and R21**Y** (5′-d(CAGAGCGTCA**Y**TCCAATGGGC)-3′) (**Y** = A, C, G and T) (Fig. 1), and other 25-mer complementary DNA oligonucleotides, F25**Z** (5′-d(GCCCTGCCTGTC**Z**CCCAGATCACTG)-3′) (**Z** = A, C, G and T) (Fig. 1) and R25**W** (5′-d(CAGTGATCTGGG**W**GACAGGCAGGGC)-3′) (**W** = A, C, G and T) (Fig. 1), using a DNA synthesizer by a solid-phase cyanoethyl phosphoramidite method. The oligonucleotides were purified by reverse-phase high-performance liquid chromatography (HPLC) on a Wakosil DNA column. The concentration of all purified oligonucleotides was determined by UV absorbance. The complementary strands, F21**X** (**X** = A, C, G and T) and R21**Y** (**Y** = A, C, G and T), and other complementary strands, F25**Z** (**Z** = A, C, G and T) and R25**W** (**W** = A, C, G and T), were annealed by heating up to 90 °C, followed by gradual cooling to room temperature. The annealed sample was applied on a hydroxyapatite column (Bio-Rad Inc., Hercules, CA, USA) to remove the unpaired single strands. The concentration of the duplex DNAs, F21**X**:R21**Y** and F25**Z**:R25**W**, was determined by UV absorption, assuming that an absorbance of 1.0 at 260 nm corresponds to 50 μg ml^{-1}.

```
F21X: 5'-d(GCCCATTGGAXTGACGCTCTG)-3'
R21Y: 3'-d(CGGGTAACCTYACTGCGAGAC)-5'        + Ag+
(X-Y=A-A, A-C, A-G, A-T, C-A, C-C, C-G, C-T,
G-A, G-C, G-G, G-T, T-A, T-C, T-G, and T-T)
 ⟶ Binding or no binding?
F25Z: 5'-d(GCCCTGCCTGTCZCCCAGATCACTG)-3'
R25W: 3'-d(CGGGACGGACAGWGGGTCTAGTGAC)-5'    + Ag+
(Z-W=A-A, A-C, A-G, A-T, C-A, C-C, C-G, C-T,
G-A, G-C, G-G, G-T, T-A, T-C, T-G, and T-T)
 ⟶ Binding or no binding?
```

Fig. 1 Examination of the present study. Possibility of the binding between Ag^+ and oligonucleotide sequences of the duplex DNA, F21**X**:R21**Y** (**X–Y** = A–A, A–C, A–G, A–T, C–A, C–C, C–G, C–T, G–A, G–C, G–G, G–T, T–A, T–C, T–G, and T–T), or F25**Z**:R25**W** (**Z–W** = A–A, A–C, A–G, A–T, C–A, C–C, C–G, C–T, G–A, G–C, G–G, G–T, T–A, T–C, T–G, and T–T), was examined in the present study.

UV melting

UV melting experiments were carried out using a DU-640 spectrophotometer (Beckman Inc., Brea, CA, USA) equipped with a Peltier cell holder. The cell path length was 1 cm. The UV melting profiles were measured in 10 mM sodium cacodylate–cacodylic acid (pH 6.8) and 100 mM $NaClO_4$ (buffer A) without or with 1 μM $AgNO_3$ at a scan rate of 0.2 °C min^{-1} with detection at 260 nm. The peak temperatures for the first derivative calculated from the UV melting profile were designated as T_m. The concentration of the duplex DNAs, F21**X**:R21**Y** and F25**Z**:R25**W**, was 1 μM. Since the water solubility of AgCl is very low, buffers containing NaCl are not suitable for the present study involving Ag^+. Instead, a buffer containing $NaClO_4$ (buffer A) was chosen in the present study due to the high water solubility of $AgClO_4$.

CD spectroscopy

CD spectra were recorded at 25 °C in buffer A (see the section UV melting) without or with 1 μM $AgNO_3$ using a JASCO J-725 spectropolarimeter interfaced with a microcomputer. The cell path length was 1 cm. The concentration of the duplex DNAs, F21**X**:R21**Y** and F25**Z**:R25**W**, was 1 μM.

Isothermal titration calorimetry (ITC)

ITC experiments were carried out using the Microcal ITC200 system (Malvern Inc., Malvern, UK). The duplex DNA solutions were prepared by extensive dialysis against buffer A (see the section UV melting). $AgNO_3$ was dissolved in the dialysis buffer. The $AgNO_3$ solution in buffer A was injected 20 times in 2 μl increments at 3 min intervals at 25 °C into the duplex DNA solutions without changing the reaction conditions. The heat for each injection was subtracted by the heat of dilution of the injectant, which was measured by injecting the $AgNO_3$ solution into the same buffer. Each corrected heat value was divided by the moles of $AgNO_3$ injected and analyzed using Microcal Origin supplied by the manufacturer.

Results

UV melting analyses of duplex DNA containing each single mismatched base pair and the corresponding perfectly matched base pair without or with Ag^+

Previous studies have reported that the T_m values of duplex DNA with each of the C–A, C–C and C–T mismatched base pairs increased upon the addition of Ag^+, although the magnitude of the increase was the highest in the case of the C–C mismatched base pair.[24] To examine whether the similar increase of the T_m values in the case of C–A, C–C and C–T mismatched base pairs upon the addition of Ag^+ is observed in the other base sequences, the thermal stability of a series of duplex DNAs, F21**X**:R21**Y** (**X–Y** = C–A, C–C, C–G and C–T) (Fig. 1), was examined in 10 mM sodium cacodylate–cacodylic acid (pH 6.8) and 100 mM $NaClO_4$ (buffer A) either without or with $AgNO_3$ by UV melting (Table 1). Without $AgNO_3$, the T_m value of the F21C:R21G duplex DNA (68.9 °C) with the perfectly

 This journal is © The Royal Society of Chemistry 2023

Open Access Article. Published on 25 August 2023. Downloaded on 1/9/2026 1:16:45 PM. This article is licensed under a Creative Commons Attribution-NonCommercial 3.0 Unported Licence.

Table 1 Melting temperatures (T_m) of 1 μM duplex DNA [F21X:R21Y (X–Y = C–A, C–C, C–G and C–T)] at pH 6.8 in 10 mM sodium cacodylate–cacodylic acid and 100 mM $NaClO_4$ without or with 1 or 2 μM $AgNO_3$, obtained from UV melting

X–Y	T_m (−Ag^+) (°C)	T_m (+Ag^+) (°C)	ΔT_m [a] (°C)	T_m (+2Ag^+) (°C)	ΔT_{m2} [b] (°C)
C–A	59.2 ± 0.1	61.3 ± 0.2	2.1	62.2 ± 0.3	3.0
C–C	57.5 ± 0.7	60.3 ± 0.7	2.8	63.0 ± 0.8	5.5
C–G	68.9 ± 0.8	70.0 ± 0.9	1.1	71.8 ± 0.8	2.9
C–T	58.7 ± 0.6	60.6 ± 0.8	1.9	62.5 ± 0.6	3.8

[a] $\Delta T_m = T_m$ (+Ag^+) − T_m (−Ag^+). [b] $\Delta T_{m2} = T_m$ (+2Ag^+) − T_m (−Ag^+).

matched C–G was significantly higher than those of the F21C:R21A, F21C:R21C, and F21C:R21T duplex DNAs with a single mismatched base pair (Table 1). The addition of $AgNO_3$ significantly increased the T_m values of all duplex DNA samples. It should be noted that the magnitude of the increase in T_m by the addition of $AgNO_3$ was the highest in the case of F21C:R21C (Table 1). These results indicated that the thermal stability of duplex DNA increased substantially and the F21C:R21C duplex DNA was the most highly stabilized by the addition of Ag^+.

In addition, the thermal stability of a series of duplex DNAs, F21**X**:R21**Y** with the 12 other base pairs (**X–Y** = A–A, A–C, A–G, A–T, G–A, G–C, G–G, G–T, T–A, T–C, T–G, and T–T) (Fig. 1), was examined in buffer A either without or with $AgNO_3$ by UV melting (Table S1†). The addition of Ag^+ increased the T_m values of all duplex DNA samples. Combination of the results of Table 1 and Table S1† indicated that in all of the 16 base pairs, the case of the C–C base pair was the most highly stabilized by the addition of Ag^+.

To investigate the effect of the addition of other metal ions on the thermal stability of duplex DNA, a series of duplex DNAs, F21**X**:R21**Y** with 16 base pairs (**X–Y** = A–A, A–C, A–G, A–T, C–A, C–C, C–G, C–T, G–A, G–C, G–G, G–T, T–A, T–C, T–G, and T–T) (Fig. 1), was examined in buffer A either without or with $Mn(NO_3)_2$, $Co(NO_3)_2$, $Ni(NO_3)_2$, $Zn(NO_3)_2$, $Cd(NO_3)_2$, $TlNO_3$, and $Pb(NO_3)_2$ by UV melting (Tables S2–S8†). The T_m values of the duplex DNA samples with any kind of base pair were not significantly changed by the addition of Mn^{2+}, Co^{2+}, Ni^{2+}, Zn^{2+}, Cd^{2+}, Tl^+, and Pb^{2+}.

To reveal whether the similar stabilization by the addition of Ag^+ is observed in the duplex DNAs with other base sequences and lengths, the thermal stability of a series of duplex DNAs with other base sequences and lengths, F25**Z**:R25**W** (**Z–W** = A–A, A–C, A–G, A–T, C–A, C–C, C–G, C–T, G–A, G–C, G–G, G–T, T–A, T–C, T–G, and T–T) (Fig. 1), was examined in buffer A either without or with $AgNO_3$ by UV melting (Table S9†). By the addition of Ag^+, the T_m values of all of the 16 duplex DNA samples were increased, and the case of the C–C base pair was the most highly stabilized, which is quite similar to the results obtained from F21**X**:R21**Y**. We conclude that, although all of the duplex DNAs were stabilized by the addition of Ag^+, the case of the C–C base pair was the most highly stabilized.

CD spectroscopy of duplex DNA containing each single mismatched base pair and the corresponding perfectly matched base pair without or with Ag^+

To examine the effect of Ag^+ on the higher-order structure of duplex DNA, the CD spectra of the two above-described series of 1 μM duplex DNA, F21**X**:R21**Y** (**X–Y** = C–A, C–C, C–G and C–T) (Fig. 1) and F25**Z**:R25**W** (**Z–W** = C–A, C–C, C–G, and C–T) (Fig. 1), were measured in buffer A (see the section UV melting) without or with 1 μM $AgNO_3$ at 25 °C (Fig. 2 and Fig. S1†). The CD profiles of each duplex DNA with $AgNO_3$ were quite similar to those observed without $AgNO_3$. These results indicated that there was no significant change in the higher-order structure of all duplex DNA upon the addition of Ag^+.

ITC analyses of the interaction between Ag^+ and each of the C–C mismatched base pair duplex DNAs and the corresponding C–G perfectly matched duplex DNAs

To explore the mechanism underlying the high stabilization of the F21C:R21C duplex DNA (Fig. 1) by the addition of Ag^+ (Table 1), we examined the thermodynamic properties of the interaction between $AgNO_3$ and F21C:R21C duplex DNA in buffer A (see the section UV melting) at 25 °C by ITC (Fig. 3). Fig. 3a shows a typical ITC profile of the interaction between $AgNO_3$ and F21C:R21C. An exothermic heat pulse was observed each time $AgNO_3$ was injected into F21C:R21C. The magnitude of each peak decreased gradually with each new injection, and a peak was still observed at the molar ratio of the last injection. The area under each peak was integrated, and the heat of the dilution of $AgNO_3$ measured in a separate experiment by injecting $AgNO_3$ into buffer A (see the section UV melting) was subtracted from the integrated values. The corrected heat was divided by the moles of the injected solution. The resulting values were plotted as a function of a molar ratio of [Ag^+]/[F21C:R21C] (circles in Fig. 3c). The resultant titration plot was sigmoidal, indicating that Ag^+ specifically bound to F21C:R21C.

To explore the mechanism underlying the stabilization of the F21C:R21G duplex DNA (Fig. 1) by the addition of Ag^+, we investigated the thermodynamic properties of the interaction between $AgNO_3$ and F21C:R21G duplex DNA in buffer A (see the section UV melting) at 25 °C by ITC (Fig. 3). Fig. 3b shows a typical ITC profile for the interaction between $AgNO_3$ and F21C:R21G. Although an exothermic heat pulse was observed after each injection of $AgNO_3$ into F21C:R21G, the magnitude of each peak did not change significantly after each new injection, in sharp contrast with the ITC profile observed for the interaction between $AgNO_3$ and F21C:R21C (Fig. 3a). The titration plot obtained from Fig. 3b (triangles in Fig. 3c) in the same way as that obtained from Fig. 3a (circles in Fig. 3c) was not sigmoidal, indicating that Ag^+ bound nonspecifically to F21C:R21G.

The nonspecific binding between Ag^+ and F21C:R21G judged from the ITC titration plots (triangles in Fig. 3c) may be explained by the electrostatic attraction between the positive

Open Access Article. Published on 25 August 2023. Downloaded on 1/9/2026 1:16:45 PM.
This article is licensed under a Creative Commons Attribution-NonCommercial 3.0 Unported Licence.

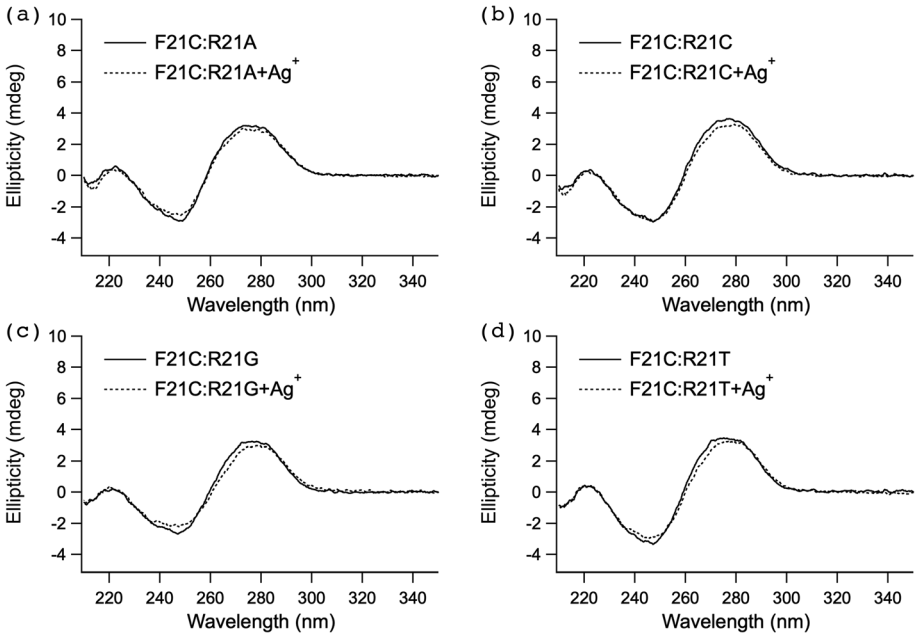

Fig. 2 CD spectra of the duplex DNA, F21C:R21A (a), F21C:R21C (b), F21C:R21G (c), and F21C:R21T (d), without or with $AgNO_3$. Duplex DNAs (1 μM) at 25 °C and pH 6.8 in buffer A (see the section UV melting) without or with 1 μM $AgNO_3$ were measured at a wavelength of 210–350 nm. The cell path length was 1 cm.

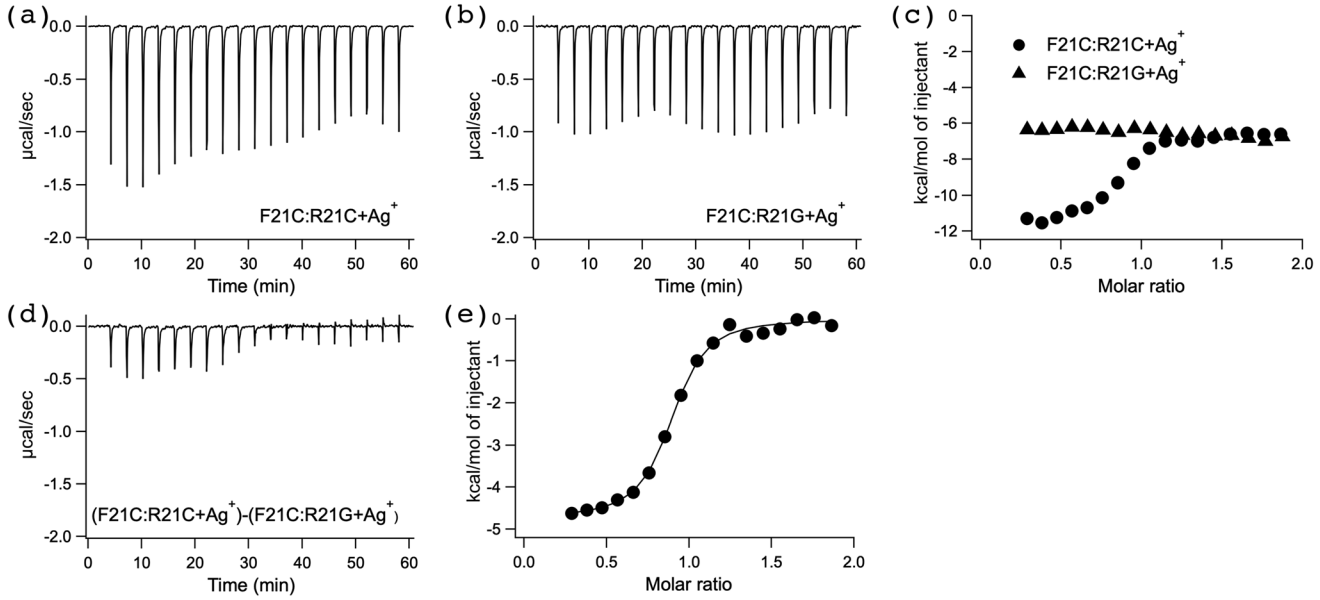

Fig. 3 Thermodynamic analyses of the interaction between Ag^+ and each of the C–C mismatches (F21C:R21C) and the perfectly matched duplex DNA (F21C:R21G). (a and b) Typical ITC profile for the interaction between $AgNO_3$ and F21C:R21C (a) and F21C:R21G (b) at 25 °C and pH 6.8 in buffer A (see the section UV melting). $AgNO_3$ solution (800 μM in buffer A) was injected 20 times in 2 μl increments into each of the F21C:R21C (a) and F21C:R21G (b) solutions (80 μM in buffer A). Injections were administered over 4 s at 3 min intervals. (c) Titration plots against the molar ratio of [Ag^+]/[duplex DNA], obtained from the ITC profiles in (a) and (b). (d) ITC profile for the binding between Ag^+ and the C–C mismatched base pair, obtained by subtracting the ITC profile observed for F21C:R21G in (b) from that observed for F21C:R21C in (a). (e) Titration plot against the molar ratio of [Ag^+]/[duplex DNA], obtained from the ITC profile in (d). The data were fitted by a nonlinear least-squares method.

charge of Ag^+ and the negative charge of the DNA phosphate backbones. In contrast, the specific binding between Ag^+ and F21C:R21C judged from the ITC titration plot (circles in Fig. 3c) suggests that Ag^+ binds specifically to the C–C mismatched base pair of F21C:R21C in addition to the nonspecific binding between Ag^+ and the DNA phosphate backbones of

Open Access Article. Published on 25 August 2023. Downloaded on 1/9/2026 1:16:45 PM. This article is licensed under a Creative Commons Attribution-NonCommercial 3.0 Unported Licence.

Table 2 Thermodynamic parameters for the specific binding between Ag^+ and the C–C mismatched base pair at 25 °C and pH 6.8 in 10 mM sodium cacodylate–cacodylic acid and 100 mM $NaClO_4$, obtained from ITC measurements

Profile	N	K_a (M^{-1})	ΔG (kcal mol^{-1})	ΔH (kcal mol^{-1})	ΔS (cal mol^{-1} K^{-1})
Fig. 3e	0.96 ± 0.01	$(9.18 \pm 1.17) \times 10^5$	−8.13 ± 0.08	−4.74 ± 0.07	11.4 ± 0.5
Fig. S2e†	1.06 ± 0.03	$(5.86 \pm 1.29) \times 10^5$	−7.87 ± 0.15	−2.37 ± 0.07	18.4 ± 0.7

F21C:R21C. Thus, the net heat derived from the specific binding between Ag^+ and the C–C mismatched base pair of F21C:R21C should be estimated by subtracting the heat observed for F21C:R21G from that observed for F21C:R21C. Accordingly, to analyze the thermodynamic parameters of the specific binding between Ag^+ and the C–C mismatched base pair of F21C:R21C, the ITC profile observed for F21C:R21G in Fig. 3b was subtracted from that observed for F21C:R21C in Fig. 3a to obtain the profile shown in Fig. 3d. The area under each peak in Fig. 3d was integrated, and the integrated values were divided by the moles of the injected solution. The resulting values were plotted as a function of the molar ratio of [Ag^+]/[duplex DNA] (Fig. 3e). The resultant titration plot was fitted to a sigmoidal curve by a nonlinear least-squares method. The stoichiometry (n), binding constant (K_a) and the enthalpy change (ΔH) for the specific binding between Ag^+ and the C–C mismatched base pair were obtained from the fitted curve.[23] The Gibbs free energy change (ΔG) and the entropy change (ΔS) were calculated from the equation $\Delta G = -RT \ln K_a = \Delta H - T\Delta S$, where R is the gas constant and T is the temperature.[23]

Table 2 summarizes the thermodynamic parameters for the specific binding between Ag^+ and the C–C mismatched base pair, obtained from Fig. 3e. The obtained value of n was nearly 1, indicating that Ag^+ bound to the C–C mismatched base pair at a molar ratio of 1 : 1. Although the sign of ΔH was negative, the sign of ΔS was positive. Both the observed negative ΔH and positive ΔS were favorable for the specific binding between Ag^+ and the C–C mismatched base pair. The magnitudes of the observed K_a and ΔG were significantly larger than those previously reported for the nonspecific interaction between metal ions and duplex DNA,[9–14] indicating that Ag^+ specifically bound to the C–C mismatched base pair in duplex DNA.

Furthermore, to investigate whether the similar specific binding of Ag^+ to the C–C mismatched base pair is observed in the duplex DNAs with other base sequences and lengths, we examined the thermodynamic properties of the interaction between $AgNO_3$ and each of the F25C:R25C and F25C:R25G duplex DNAs in buffer A (see the section UV melting) at 25 °C by ITC (Fig. S2†). Fig. S2a and S2b† show typical ITC profiles of the interaction between $AgNO_3$ and each of the F25C:R25C and F25C:R25G duplex DNAs, respectively. Although the titration plot obtained from Fig. S2b† (triangles in Fig. S2c†) was not sigmoidal, that obtained from Fig. S2a† (circles in Fig. S2c†) was sigmoidal. The ITC profile observed for F25C:R25G in Fig. S2b† was subtracted from that observed for F25C:R25C in Fig. S2a† to obtain the profile shown in Fig. S2d,† which corresponds to only the specific binding between Ag^+ and the C–C mismatched base pair. The titration plot obtained from Fig. S2d† (Fig. S2e†) was fitted to a sigmoidal curve by a nonlinear least-squares method to obtain the thermodynamic parameters of the specific binding between Ag^+ and the C–C mismatched base pair of F25C:R25C (Table 2). The thermodynamic parameters obtained from Fig. S2e† were similar in magnitude to those obtained from Fig. 3e (Table 2). The difference of the base sequences and lengths of the C–C mismatched duplex DNA did not significantly influence the thermodynamic parameters of the specific binding between Ag^+ and the C–C mismatched base pair.

ITC analyses of the interaction between Ag^+ and each of the C–A and C–T mismatched base pair duplex DNAs

To examine the mechanism underlying the stabilization of the F21C:R21A and F21C:R21T duplex DNAs (Fig. 1) by the addition of Ag^+ (Table 1), we investigated the thermodynamic properties of the interaction between $AgNO_3$ and each of the F21C:R21A and F21C:R21T duplex DNAs in buffer A (see the section UV melting) at 25 °C by ITC (Fig. 4). Fig. 4a and c show typical ITC profiles for the interaction between $AgNO_3$ and each of the F21C:R21A and F21C:R21T DNAs, respectively. Although an exothermic heat pulse was observed after each injection of $AgNO_3$ into F21C:R21A and F21C:R21T, the magnitude of each peak did not change significantly after each new injection, in sharp contrast to the ITC profile observed for the interaction between $AgNO_3$ and F21C:R21C (Fig. 3a). The titration plots obtained from Fig. 4a for F21C:R21A (circles in Fig. 4b) and Fig. 4c for F21C:R21T (circles in Fig. 4d), as in Fig. 3c, were not sigmoidal, and they were quite similar in magnitude to the titration plot obtained from Fig. 3b for F21C:R21G (triangles in Fig. 3c, 4b and d), indicating that Ag^+ showed nonspecific binding to F21C:R21A and F21C:R21T. The nonspecific binding between Ag^+ and each of the F21C:R21A and F21C:R21T DNAs judged from the ITC titration plots (circles in Fig. 4b and d) may be attributed to the electrostatic attraction between the positive charge of Ag^+ and the negative charge of the DNA phosphate backbones, similar to the case of perfectly matched F21C:R21G (triangles in Fig. 3c, 4b and d). In conclusion, the ITC titration plots for the C–A (circles in Fig. 4b) and C–T (circles in Fig. 4d) mismatched duplex DNAs indicated that Ag^+ may not bind to the C–A and C–T mismatched base pairs of the duplex DNA, although it may bind to the phosphate backbones of the duplex DNA.

Open Access Article. Published on 25 August 2023. Downloaded on 1/9/2026 1:16:45 PM.
This article is licensed under a Creative Commons Attribution-NonCommercial 3.0 Unported Licence.

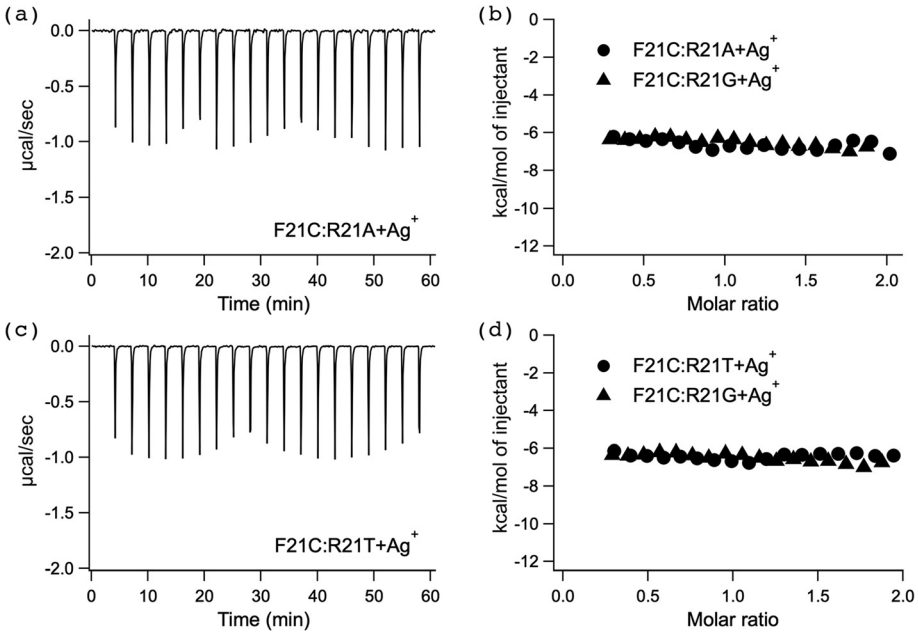

Fig. 4 Thermodynamic analyses of the interaction between Ag^+ and the C–A or C–T mismatches (F21C:R21A or F21C:R21T) or the perfectly matched (F21C:R21G) duplex DNA. (a) Typical ITC profile for the interaction between $AgNO_3$ and F21C:R21A at 25 °C and pH 6.8 in buffer A (see the section UV melting). $AgNO_3$ solution (800 μM in buffer A) was injected 20 times in 2 μl increments into F21C:R21A solution (80 μM in buffer A). Injections were administered over 4 s at 3 min intervals. (b) Titration plot against the molar ratio of [Ag^+]/[duplex DNA], obtained from the ITC profiles for F21C:R21A in (a) and for F21C:R21G (triangles in Fig. 3c). (c) Typical ITC profile for the interaction between $AgNO_3$ and F21C:R21T at 25 °C and pH 6.8 in buffer A (see the section UV melting). $AgNO_3$ solution (800 μM in buffer A) was injected 20 times in 2 μl increments into F21C:R21T solution (80 μM in buffer A). Injections were administered over 4 s at 3 min intervals. (d) Titration plot against the molar ratio of [Ag^+]/[duplex DNA], obtained from the ITC profiles for F21C:R21T in (c) and for F21C:R21G (triangles in Fig. 3c).

Discussion

UV melting analyses showed that among mismatches, the C–C mismatched base pair (F21C:R21C and F25C:R25C) was most highly stabilized by the addition of Ag^+ (Tables 1, S1 and S9†). We previously reported that a C–C mismatch in duplex DNA with another base sequence was also highly stabilized by the Ag^+ addition,[24,26,30] consistent with the present results. ITC analyses (Fig. 3, Fig. S2,† and Table 2) showed that Ag^+ may specifically bind to the C–C mismatched base pair of the duplex DNA in addition to nonspecific binding between Ag^+ and the DNA phosphate backbones of the duplex DNA, although only the nonspecific binding between Ag^+ and the DNA phosphate backbones was observed for the other duplex DNA. The two types of the binding may explain the high stability of the C–C mismatch in duplex DNAs (F21C:R21C and F25C:R25C) upon the addition of Ag^+. These results demonstrated that Ag^+ may stabilize the C–C mismatched base pair in duplex DNA by direct binding to the mismatched base pair.

ITC analyses of the interaction between Ag^+ and the C–C mismatched base pairs (F21C:R21C and F25C:R25C) revealed that Ag^+ bound to the C–C mismatched base pair in the duplex DNA at a molar ratio of 1 : 1 (Fig. 3, Fig. S2,† and Table 2). The K_a and ΔG values for the specific binding between Ag^+ and the C–C mismatched base pair were nearly 10^6 M^{-1} and −8.13 or −7.87 kcal mol^{-1}, respectively (Table 2). These values were significantly greater than previously reported estimates for the nonspecific interaction between metal ions and DNA,[9–14] supporting the specific binding between Ag^+ and the C–C mismatched base pair. The observed ΔG resulted from both the negative ΔH and positive ΔS (Table 2). The positive ΔS for the specific binding between Ag^+ and the C–C mismatched base pair measured by ITC (Table 2) can be explained, in large part, by a positive dehydration entropy change from the release of structured water molecules surrounding Ag^+ and the duplex DNA and a conformational entropy change derived from the conformational change of the duplex DNA upon binding to Ag^+. The CD spectra showed that the higher-order structure of the duplex DNA was not significantly distorted by the specific binding of Ag^+ (Fig. 2), suggesting that the conformational entropy change did not contribute substantially to the observed positive ΔS (Table 2). Thus, the positive ΔS (Table 2) may result mainly from the positive dehydration entropy change from the release of structured water molecules surrounding Ag^+ and the duplex DNA. In fact, a previously reported positive dehydration entropy change of Ag^+ (18 cal mol^{-1} K^{-1})[39] was similar in magnitude to the observed positive ΔS (Table 2). The negative ΔH for the specific binding between Ag^+ and the C–C mismatched base pair measured by ITC (Table 2) reflects the positive dehydration enthalpy change of Ag^+,[40] and a negative binding enthalpy change derived from the bond formation between Ag^+ and the Ag^+ binding positions in the two cytosine bases to form the C–Ag–C metal-mediated base pair. Since the sign of the binding enthalpy change upon

 This journal is © The Royal Society of Chemistry 2023

Open Access Article. Published on 25 August 2023. Downloaded on 1/9/2026 1:16:45 PM.
This article is licensed under a Creative Commons Attribution-NonCommercial 3.0 Unported Licence.

bond formation was negative and the sign of the dehydration enthalpy change was positive, the observed negative ΔH (Table 2) might have been driven mainly by the negative binding enthalpy change upon the bond formation of the C–Ag–C metal-mediated base pair. Based on these findings, we propose a possible scheme for the specific binding between Ag^+ and the C–C mismatched base pair (Fig. 5). Ag^+ surrounded by structured water molecules may be dehydrated, and this may be closely related to the positive dehydration entropy change. The dehydrated Ag^+ may bind to the two cytosine bases to form the C–Ag–C metal-mediated base pair, and this may be closely related to the negative binding enthalpy change.

UV melting analyses showed that the addition of Ag^+ increased the T_m of the C–A (F21C:R21A) and C–T (F21C:R21T) mismatched base pairs in duplex DNA (Table 1). These findings were consistent with our previous analyses, showing that the C–A and C–T mismatches in duplex DNA with other base sequences were also highly stabilized by the Ag^+ addition.[30] The increase in the T_m of duplex DNA with mismatched base pairs upon the addition of metal ions frequently results from direct binding of the metal ions to the mismatched base pair. In fact, T_m for the T–T mismatch in duplex DNA increased upon the addition of Hg^{2+} due to direct binding.[15,16,18] However, in ITC analyses of the interaction between Ag^+ and the C–A and C–T mismatches, the titration plots for F21C:R21A (circles in Fig. 4b) and for F21C:R21T (circles in Fig. 4d) were quite similar in magnitude to that for the perfectly matched duplex DNA (F21C:R21G) (triangles in Fig. 3c, 4b and d). These results indicate that the positive charge of Ag^+ may bind to the negative charge of the phosphate backbones of F21C:R21A and F21C:R21T in a nonspecific manner without the specific binding to the C–A and C–T mismatches of F21C:R21A and F21C:R21T. The nonspecific interaction between the positive charge of Ag^+ and the negative charge of the phosphate backbones of F21C:R21A and F21C:R21T may increase the T_m value and the thermal stability of F21C:R21A and F21C:R21T.

UV melting analyses are often used to examine the binding of metal ions to the mismatched base pair in duplex DNA.[31–38]

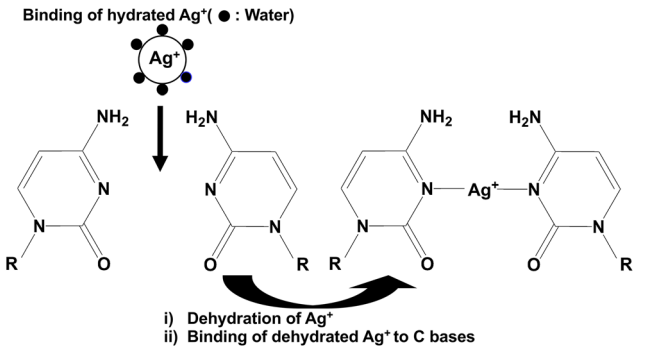

Fig. 5 Proposed scheme for the specific binding between Ag^+ and the C–C mismatched base pair. Hydrated Ag^+ surrounded by structured water molecules may be dehydrated. The dehydrated Ag^+ may bind to the two cytosine bases to form an N3–Ag–N3 bond.

The increase in T_m observed by UV melting analyses may result from stabilization by the two types of the binding: (1) the specific binding between metal ions and mismatched base pairs and (2) the nonspecific binding between the positive charge of metal ions and the negative charge of DNA phosphate backbones of the duplex DNA. Since UV melting analyses of the change in the thermal stability of the duplex DNA are unable to capture the direct binding between metal ions and mismatches in duplex DNA, they cannot be used to discriminate between the two types of the binding. On the other hand, because ITC analyses directly detect the heat derived from binding,[23] they can be used to discriminate between the two types of binding. Accordingly, we conclude that ITC analyses may be more effective than UV melting analyses for the detection of the specific binding of metal ions to the mismatched base pairs in duplex DNA.

Conclusions

Our results demonstrated that Ag^+ binds specifically to the C–C mismatched base pair of the duplex DNA without binding to the C–A and C–T mismatched base pairs, although Ag^+ may bind to the phosphate backbones of the duplex DNA nonspecifically. Furthermore, the T_m value of the mismatched duplex DNA increased upon the addition of metal ions, even when the metal ions were unable to bind to the mismatched base pair, as in the case of the C–A and C–T mismatches. Thus, the increase in the T_m of the mismatched duplex DNA upon the addition of metal ions cannot be used to detect the specific binding between the metal ion and the mismatched base pair. Alternatively, by the direct detection of the heat derived from the binding between the metal ions and the mismatched base pair,[23] ITC analyses can be used to evaluate specific binding. UV melting analyses are often used to propose novel binding schemes between metal ions and an artificially designed mismatched base pair of the duplex DNA.[31–38] Owing to the low reliability of UV melting analyses, previously proposed binding schemes between metal ions and artificially designed mismatched base pairs should be reexamined by ITC analyses. The formation of metal-mediated base pairs by the specific binding between metal ions and mismatches has various types of applications,[22] including applications in metal (Hg^{2+} and Ag^+) sensors, Hg^{2+} trapping, single nucleotide polymorphism detection, and DNA nanomachines (DNA tweezers, DNA walkers and logic gates). Taken together, we conclude that ITC analyses are important for the detection of the specific binding of metal ions to mismatched base pairs in duplex DNA and may expand the applications of metal-mediated base pairs in various fields.

Conflicts of interest

The authors declare no conflict of interest.

Open Access Article. Published on 25 August 2023. Downloaded on 1/9/2026 1:16:45 PM.
This article is licensed under a Creative Commons Attribution-NonCommercial 3.0 Unported Licence.

Acknowledgements

This work was supported in part by the Grant-in-Aid for Challenging Exploratory Research (18K19308) and the Grant-in-Aid for Scientific Research (B) (17H03033) from the Japan Society for the Promotion of Science.

References

1 Y. Hu, A. Cecconello, A. Idili, F. Ricci and I. Willner, *Angew. Chem., Int. Ed.*, 2017, **56**, 15210–15233.
2 S. Naskar, R. Guha and J. Muller, *Angew. Chem., Int. Ed.*, 2020, **59**, 1397–1406.
3 M. Nishio, K. Tsukakoshi and K. Ikebukuro, *Biosens. Bioelectron.*, 2021, **178**, 113030.
4 P. J. Huang and J. Liu, *ChemistryOpen*, 2020, **9**, 1046–1059.
5 L. Ma and J. Liu, *iScience*, 2020, **23**, 100815.
6 R. Saran, Y. Wang and I. T. S. Li, *Sensors*, 2020, **20**, 7019.
7 A. Heuer-Jungemann and V. Linko, *ACS Cent. Sci.*, 2021, **7**, 1969–1979.
8 S. Lu, J. Shen, C. Fan, Q. Li and X. Yang, *Adv. Sci.*, 2021, **8**, 2100328.
9 H. Arakawa, R. Ahmad, M. Naoui and H. A. Tajmir-Riahi, *J. Biol. Chem.*, 2000, **275**, 10150–10153.
10 A. A. Ouameur, S. Nafisi, N. Mohajerani and H. A. Tajmir-Riahi, *J. Biomol. Struct. Dyn.*, 2003, **20**, 561–565.
11 A. A. Ouameur, H. Arakawa, R. Ahmad, M. Naoui and H. A. Tajmir-Riahi, *DNA Cell Biol.*, 2005, **24**, 394–401.
12 J. Wu, F. Du, P. Zhang, I. A. Khan, J. Chen and Y. Liang, *J. Inorg. Biochem.*, 2005, **99**, 1145–1154.
13 Y. Li, Y. L. Xia, Y. Jiang and X. P. Yan, *Electrophoresis*, 2008, **29**, 1173–1179.
14 K. Utsuno, *Chem. Pharm. Bull.*, 2008, **56**, 247–249.
15 A. Ono and H. Togashi, *Angew. Chem., Int. Ed.*, 2004, **43**, 4300–4302.
16 Y. Miyake, H. Togashi, M. Tashiro, H. Yamaguchi, S. Oda, M. Kudo, Y. Tanaka, Y. Kondo, R. Sawa, T. Fujimoto, T. Machinami and A. Ono, *J. Am. Chem. Soc.*, 2006, **128**, 2172–2173.
17 Y. Tanaka, S. Oda, H. Yamaguchi, Y. Kondo, C. Kojima and A. Ono, *J. Am. Chem. Soc.*, 2007, **129**, 244–245.
18 H. Torigoe, A. Ono and T. Kozasa, *Chemistry*, 2010, **16**, 13218–13225.
19 A. Ono, H. Torigoe, Y. Tanaka and I. Okamoto, *Chem. Soc. Rev.*, 2011, **40**, 5855–5866.
20 H. Torigoe, Y. Miyakawa, A. Ono and T. Kozasa, *Thermochim. Acta*, 2012, **532**, 28–35.
21 J. Kondo, T. Yamada, C. Hirose, I. Okamoto, Y. Tanaka and A. Ono, *Angew. Chem., Int. Ed.*, 2014, **53**, 2385–2388.
22 Y. Tanaka, J. Kondo, V. Sychrovsky, J. Sebera, T. Dairaku, H. Saneyoshi, H. Urata, H. Torigoe and A. Ono, *Chem. Commun.*, 2015, **51**, 17343–17360.
23 T. Wiseman, S. Williston, J. F. Brandts and L. N. Lin, *Anal. Biochem.*, 1989, **179**, 131–137.
24 A. Ono, S. Cao, H. Togashi, M. Tashiro, T. Fujimoto, T. Machinami, S. Oda, Y. Miyake, I. Okamoto and Y. Tanaka, *Chem. Commun.*, 2008, 4825–4827, DOI: **10.1039/b808686a**.
25 H. Torigoe, Y. Miyakawa, A. Ono and T. Kozasa, *Nucleosides, Nucleotides Nucleic Acids*, 2011, **30**, 149–167.
26 H. Torigoe, I. Okamoto, T. Dairaku, Y. Tanaka, A. Ono and T. Kozasa, *Biochimie*, 2012, **94**, 2431–2440.
27 J. Kondo, Y. Tada, T. Dairaku, H. Saneyoshi, I. Okamoto, Y. Tanaka and A. Ono, *Angew. Chem., Int. Ed.*, 2015, **54**, 13323–13326.
28 T. Dairaku, K. Furuita, H. Sato, J. Sebera, K. Nakashima, J. Kondo, D. Yamanaka, Y. Kondo, I. Okamoto, A. Ono, V. Sychrovsky, C. Kojima and Y. Tanaka, *Chemistry*, 2016, **22**, 13028–13031.
29 J. Kondo, Y. Tada, T. Dairaku, Y. Hattori, H. Saneyoshi, A. Ono and Y. Tanaka, *Nat. Chem.*, 2017, **9**, 956–960.
30 T. Funai, M. Aotani, R. Kiriu, J. Nakamura, Y. Miyazaki, O. Nakagawa, S. I. Wada, H. Torigoe, A. Ono and H. Urata, *ChemBioChem*, 2020, **21**, 517–522.
31 H. Urata, E. Yamaguchi, Y. Nakamura and S. Wada, *Chem. Commun.*, 2011, **47**, 941–943.
32 T. Richters, O. Krug, J. Kosters, A. Hepp and J. Muller, *Chem. – Eur. J.*, 2014, **20**, 7811–7818.
33 H. Z. Yang and F. Seela, *Chem. – Eur. J.*, 2016, **22**, 13336–13346.
34 X. R. Guo and F. Seela, *Chem. – Eur. J.*, 2017, **23**, 11776–11779.
35 B. Jash and J. Muller, *Chem. – Eur. J.*, 2018, **24**, 10636–10640.
36 N. Sandmann, D. Defayay, A. Hepp and J. Muller, *J. Inorg. Biochem.*, 2019, **191**, 85–93.
37 X. L. Zhou, D. Kondhare, P. Leonard and F. Seela, *Chem. – Eur. J.*, 2019, **25**, 10408–10419.
38 I. Schonrath, H. Aukam, B. Jasper-Peter and J. Muller, *Nucleosides, Nucleotides Nucleic Acids*, 2022, **41**, 23–35.
39 D. R. Rosseinsky, *Chem. Rev.*, 1965, **65**, 467–490.
40 A. A. Rashin and B. Honig, *J. Phys. Chem.*, 1985, **89**, 5588–5593.

 This journal is © The Royal Society of Chemistry 2023